Published online 31 January 2007 *Nucleic Acids Research, 2007, Vol. 35, No. 4* **1209–1221**
doi:10.1093/nar/gkl1148

CRD-BP shields c-*myc* and *MDR*-1 RNA from endonucleolytic attack by a mammalian endoribonuclease

Dan Sparanese and Chow H. Lee*

Chemistry Program, University of Northern British Columbia, 3333 University Way, Prince George, BC V2N 4Z9, Canada

Received October 9, 2006; Revised November 29, 2006; Accepted December 17, 2006

ABSTRACT

The c-*myc* mRNA coding region determinant-binding protein (CRD-BP) has high affinity for the coding region determinant (CRD) of c-*myc* mRNA. Such affinity is believed to protect c-*myc* CRD from endonucleolytic attack. We have recently purified a mammalian endoribonuclease which can cleave within the c-*myc* CRD *in vitro*. The availability of this purified endonuclease has made it possible to directly test the interaction between CRD-BP and the endonuclease in regulating c-*myc* CRD RNA cleavage. In this study, we have identified the coding region of *MDR*-1 RNA as a new target for CRD-BP. CRD-BP has the same affinity for c-*myc* CRD nts 1705–1886 and *MDR*-1 RNA nts 746–962 with K_d of 500 nM. The concentration-dependent affinity of CRD-BP to these transcripts correlated with the concentration-dependent blocking of endonuclease-mediated cleavage by CRD-BP. In contrast, three other recombinant proteins tested which had no affinity for c-*myc* CRD did not block endonuclease-mediated cleavage. Finally, we have identified RNA sequences required for CRD-BP binding. These results provide the first direct evidence that CRD-BP can indeed protect c-*myc* CRD cleavage initiated by an endoribonuclease, and the framework for further investigation into the interactions between CRD-BP, c-*myc* mRNA, *MDR*-1 mRNA and the endoribonuclease in cells.

INTRODUCTION

The c-Myc protein is an important transcription factor. It influences cell proliferation, differentiation and apoptosis via the activation of a multitude of target genes (1). It has been estimated that c-Myc can influence the expression of ~10% of all genes in humans (1). c-Myc is implicated in human cancers, and overexpression of c-Myc at the protein and/or mRNA levels has been observed in virtually all types of cancers (2). These observations highlight the significance of understanding c-*myc* gene regulation.

c-Myc expression is regulated at multiple levels including the level of mRNA stability (3–5). By using a cell-free mRNA decay assay as well as *in vivo* analysis, it has been shown that c-*myc* mRNA can be degraded by two different pathways. One pathway involves rapid removal of the poly(A) tail which is then followed by 3′–5′ decay accomplished by 3′–5′ exoribonuclease(s) (6,7). The second decay pathway involves endonucleolytic cleavage within the coding region of c-*myc* mRNA, a region termed the coding region determinant (CRD) (5). Several studies have subsequently confirmed that the coding region of c-*myc* mRNA, including the CRD, is involved in the regulation of c-*myc* mRNA stability in cells (3,8–11).

A cell-free mRNA decay assay involving polysome extracts and a 180 nt RNA sense strand corresponding to the c-*myc* CRD was found to induce endonucleolytic cleavage within the c-*myc* CRD and destabilized the transcript 8-fold (5). The effect was highly specific because competitor RNA corresponding to other regions of the c-*myc* transcript failed to destabilize c-*myc* mRNA (5). Based on these observations, Ross and co-workers (5) postulated the following model: (i) c-*myc* mRNA is susceptible to attack by a polysome-associated endoribonuclease; (ii) a protein can interact with and protect the CRD from attack by an endoribonuclease; (iii) the addition of competitor CRD RNAs titrate the protein off c-*myc* mRNA, leaving the CRD unprotected and susceptible to endonuclease attack. A protein that binds with high affinity *in vitro* to the c-*myc* CRD has been purified (12) and cloned (13). This protein termed the c-*myc* mRNA coding region determinant-binding protein or CRD-BP, was later found to be identical to the IGF-II mRNA-binding protein 1 (IMP-1) (14).

*To whom correspondence should be addressed. Tel: +250 960 5413; Fax: +250 960 5170; Email: leec@unbc.ca

The following observations supported CRD-BP being an oncofetal protein. CRD-BP has been shown to be abundantly expressed in fetal tissues but not in adult tissues (15). CRD-BP-deficient mice exhibited dwarfism, impaired gut development and increased perinatal mortality (16), providing further support that CRD-BP plays a critical role in developmental processes. *De novo* expression studies on CRD-BP have shown it to be overexpressed in breast cancer (17), colorectal cancer (18), brain tumors (19) and non-small cell lung tumors (19). Further evidence to associate CRD-BP with breast cancer are the observations that ~30% of human breast cancer cases exhibited amplification of the CRD-BP gene (20), and transgenic mice carrying targeted expression of the protein developed mammary tumors (21).

To date, CRD-BP and its orthologs have been shown to bind to several RNAs, and depending on the RNA in question, multiple functions for these proteins have been proposed. CRD-BP binds to the 5′-untranslated region of *IGF*-II mRNA and influences its subcellular localization and translation (14,22). CRD-BP also binds to *H*19 RNA (23) and neuron-specific *tau* mRNA (24) to influence their localization in cells. The zipcode-binding protein binds to β-actin mRNA and localizes it to the leading edge of fibroblast lamellipodia (25). The IMP binds to the 3′-untranslated region of CD44 mRNA and stabilizes the transcript (26). A recent study has identified CRD-BP as the protein that interacts with the coding region of βTrCP1 mRNA and stabilizes the transcript in response to the β-catenin signaling pathway (27). Finally, as indicated above, CRD-BP has been shown to bind to and is believed to shield the c-*myc* CRD from endonucleolytic attack thereby prolonging its cytosolic half-life (5).

Three observations support the CRD-BP-c-*myc* CRD shielding hypothesis. First, overexpression of CRD-BP in colorectal cancer correlates with a modest elevation of c-*myc* mRNA levels (18). Second, decreased expression of c-*myc* mRNA subsequent to knockdown of CRD-BP was observed in MCF-7 (28) and colorectal cells (27). Finally, addition of sense RNA corresponding to the CRD resulted in enhanced decay of c-*myc* mRNA in cells (29). However, the following two recent observations do not support the CRD-BP-c-*myc* CRD shielding hypothesis: (i) transgenic mice over-expressing CRD-BP in mammary tissues did not exhibit elevated levels of c-*myc* mRNA (21); and (ii) targeted knockdown of CRD-BP in K562 cells had no effect on c-*myc* mRNA levels (30). Such unexpected results or discrepancies may in part be due to the role of the third party molecule, namely an endoribonuclease that can cleave the c-*myc* CRD. The availability of an identified endoribonuclease should permit systematic testing of the CRD-BP-c-*myc* CRD shielding hypothesis *in vitro* and *in vivo*, and may help clarify some of the contradictory reports.

We have recently purified a mammalian endoribonuclease from rat liver based on its ability to cleave within the c-*myc* CRD (31). Several biochemical properties distinguished the enzyme from previously described vertebrate endonucleases and supported it being a novel mammalian endoribonuclease (31). The enzyme preferentially cleaves between the dinucleotides UA, CA and UG, and it is capable of cleaving other RNAs including *MDR*-1 and β-*globin* RNAs (31). With the availability of purified mammalian endoribonuclease and recombinant CRD-BP, we sought to directly test the CRD-BP-c-*myc* CRD-shielding hypothesis. In this study, we show that CRD-BP is able to dose-dependently bind to c-*myc* CRD RNA and *MDR*-1 RNA with K_d of ~500 nM. This interaction correlates with its ability to dose-dependently inhibit cleavage of c-*myc* CRD and *MDR*-1 RNA by the mammalian endoribonuclease.

MATERIALS AND METHODS

Expression and purification of recombinant CRD-BP, Rpp20, Rpp21, Rpp25 and Rpp40

The plasmid pET28b(+)-CRD-BP which contains mouse CRD-BP cDNA was a generous gift from Dr Jeffrey Ross, University of Wisconsin and was prepared as previously described (13). Plasmids pHTT7k-p20, pHTT7k-p21, pHTT7k-p25 and pHTT7k-p40 which contain the Rpp20, Rpp21, Rpp25 and Rpp40 cDNAs were generous gifts from Dr Sidney Altman, Yale University and were prepared as previously described (32–34). All His_6-tagged proteins were purified from *Escherichia coli* BL21(DE3) using the QIAexpress Ni-NTA metal affinity spin kit (QIAGEN) under denaturing conditions. Proteins eluted from the column at either pH 5.4 or 4.5 were subjected to a series of dialysis steps (3 h at each step) pH 5/6 M urea, pH 5.5/4 M urea, pH 6/2 M urea, pH 6.7/1M urea and pH 7.4/0 M urea in a buffer containing 200 mM KCl, 1 mM EDTA, 10% (v/v) glycerol, 1 mM reduced glutathione, 0.1 mM oxidized glutathione, 0.01% (v/v) Triton X-100, 20 mM triethanolamine (13) and EDTA-free protease inhibitor tablets (Roche). Following dialysis, samples were spun at 13,200 rpm for 30 min to remove any precipitated proteins. The purified protein solutions were then quantified and analyzed for purity using Coomasie blue-stained 12% SDS-PAGE.

Purification of the mammalian endoribonuclease

Purification of the mammalian endoribonuclease from rat livers has been previously described (31). One unit of the purified enzyme from the last step of column chromatography, the heparin-sepharose column, was used in all experiments described in this study.

In vitro transcription and labeling of 5′ ends of RNA

To synthesize c-*myc* CRD RNA, plasmids pUC19-CRD*myc*-1705-1792 (31) and pUC19-CRD*myc*-1705-1886 were linearized with EcoRI and transcribed with SP6 RNA polymerase using SP6 Megascript kits (Ambion, TX, USA). To make human β-*globin* RNA corresponding to nts 1–145, the plasmid SPκβc (35) was linearized with FokI and transcribed with SP6 RNA polymerase using SP6 Megascript kit. To make human *MDR*-1 RNA corresponding to nts 746–962, the plasmid pGEM7Z-*MDR*-1-V2 was linearized with *Apa*LI and transcribed with T7 RNA polymerase using T7 Megascript kit (Ambion, TX, USA). For 5′-^{32}P-end

labeling of RNA, 5 μg of *in-vitro* transcribed RNA was first dephosphorylated with 10 units of calf alkaline phosphatase (GE Healthcare) for 30 min at 37°C in a 100-μl reaction according to the manufacturer's instructions. Dephosphorylated RNA was purified by phenol/chloroform extraction and ethanol precipitation. About 2.5 μg of dephosphorylated RNA was incubated in a 25-μl reaction with 30–50 μCi of [γ-^{32}P] ATP at 37°C for 1 h with 40–50 units of T4 polynucleotide kinase (New England Biolabs). The entire sample was then run on a 6% polyacrylamide/7M urea gel and the band containing 5′-labeled ^{32}P-RNA was excised and eluted with elution buffer (0.5 M ammonium acetate, 1 mM EDTA, 0.2% SDS) at 37°C for 6 h. The purified radiolabeled RNA was then concentrated by ammonium acetate/isopropanol precipitation. Specific activity of the RNA was determined by scintillation counting.

Electrophoretic mobility shift assays

Electrophoretic mobility shift assay (EMSA) binding buffers (5 mM Tris-Cl pH 7.4, 2.5 mM EDTA pH 8.0, 2 mM DTT, 5% glycerol, 0.1 mg/ml bovine serum albumin, 0.5 mg/ml yeast tRNA, 5 units RNasin) (13) were prepared on ice prior to each experiment. In order to facilitate RNA denaturation and renaturation, the [^{32}P] RNA sample was heated to 50°C for 5 min and cooled to room temperature before being added to the EMSA-binding buffer. EMSA-binding buffer containing radiolabeled RNA was then incubated with purified recombinant protein in a 20-μl reaction volume at 30°C for 10 min and transferred to ice for 5 min. The reaction was again incubated at 30°C for 10 min and transferred to ice for an additional 5 min. Heparin (Sigma) was then added to a final concentration of 5 mg/ml and the reaction was incubated on ice for a final 5-min period. A total of 2 μl EMSA loading dye (250 mM Tris-Cl pH 7.4, 0.2% bromophenol blue, 0.2% xylene cyanol, 40% sucrose) was added to each reaction and 10 μl of the EMSA reaction was loaded onto an 8% native polyacrylamide gel and resolved at 25 mA for 90 min. Following electrophoresis, the gel was dried and subjected to autoradiography using the Cyclone PhosphorImager and Optiquant Software.

All EMSA saturation-binding experiments were carried out as described above and the dissociation constant (K_d) for CRD-BP against *MDR*-1 and c-*myc* CRD was determined by fits to the Hill equation:

$$\frac{\text{bound}}{\text{Total}} = \frac{\left(\frac{1}{k_d}\right)[L]^n}{1 + \left(\left(\frac{1}{k_d}\right)[L]\right)^n}$$

where K_d is the dissociation constant and $[L]$ is the concentration of CRD-BP and n is the Hill coefficient. All saturation-binding data was analyzed by densitometry of the autoradiograph using the Cyclone Storage Phosphor-System and Optiquant software. For each reaction the total activity in each lane was determined; this involved summing the total activity in bound complexes with the total activity present in the unbound fraction. It should be noted that in lanes in which both Complex I and Complex II were present, their total activity was added together and therefore represented the total bound fraction. This analysis allowed for the calculation of the percentage of RNA bound to the protein. The percentage of bound RNA and the protein concentration (nM) were inserted into the Hill equation and the results were expressed graphically.

For EMSA competition assays, 5′-[^{32}P] radiolabeled c-*myc* CRD RNA nts 1705–1886 and unlabeled *in vitro* transcribed competitor RNA were prepared as described above. EMSA-binding buffers and EMSA reaction mixtures were prepared and 350 nM of CRD-BP was added to the reactions containing one of the following unlabeled competitors: c-*myc*-CRD-1705-1885, c-*myc*-CRD 1705-1792, *MDR*-1 or β-*globin* RNA. EMSA competition assays involved the pre-incubation between competitor RNA and CRD-BP for 10 min at 30°C. Following the pre-incubation, 40 nM [^{32}P] c-*myc* CRD RNA was added to the reaction. This was followed by the standard EMSA protocol as described above. The concentrations of unlabeled competitor RNA employed were 1-, 2-, 5-, 10- and 50-fold greater than the 40 nM [^{32}P] c-*myc*-CRD RNA used.

In vitro endonuclease shielding assay

The first step of this assay involved the binding between one of the [^{32}P] RNA constructs (c-*myc* CRD-1705-1886, *MDR*-1 or β-*globin*) and one of the purified recombinant proteins (CRD-BP, Rpp20, Rpp21, Rpp25 or Rpp40). Binding was facilitated using the standard EMSA protocol. Immediately following the final EMSA step, one unit of the heparin-sepharose purified mammalian endoribonuclease was added to the binding reaction, mixed and incubated at 37°C for 3 min. As a positive control, the dialyzed mammalian endoribonuclease was added to the EMSA buffer in the absence of recombinant protein and incubated at 37°C for 3 min. All reactions were terminated by heating at 100°C for 3 min followed by the addition of 1 μl phenol and 3 μl formamide loading dye (80% formamide, 0.05 mg/ml bromophenol blue, 0.05 mg/ml xylene cyanol, 0.01 M EDTA pH 8.0). Aliquots containing ~30 000 c.p.m. were loaded onto 8% denaturing polyacrylamide gel and resolved at 30 mA until the bromophenol blue reached the bottom of the gel plate. Gels were fixed in 10% acetic acid, 10% methanol for 15 min and subjected to autoradiography. In some experiments, higher amounts (three units) of the purified endoribonuclease were used. In such cases, similar blocking effects of CRD-BP on endonuclease-mediated cleavage were observed.

RNase T1 digestion and alkaline hydrolysis of radiolabeled c-*myc* CRD RNA were performed to generate sequencing ladders for cleavage site identification purposes. Alkaline ladders were generated by combining 100 000 c.p.m. [^{32}P] c-*myc* CRD-1705-1886 RNA and 1× alkaline hydrolysis buffer (50 mM $NaHCO_3/Na_2CO_3$ pH 9.2, 1 mM EDTA, 3 μg yeast tRNA) in a total reaction volume not exceeding 15 μl. The reaction was incubated at 95°C for 10 min, transferred to ice and combined with 20 μl of formamide loading dye and stored at −20°C

until required. RNase T1 digests were generated by incubating 100 000 c.p.m. [^{32}P] c-*myc* CRD-1705-1886 RNA in EMSA-binding buffer with 1 unit of RNase T1 (Ambion). The RNA/EMSA binding buffer mixture was heated to 55°C for 5 min and cooled to room temperature prior to the addition of RNase T1. The T1 cleavage reaction was incubated at room temperature for 10 min and was terminated by phenol/chloroform extraction. The RNA was extracted using ammonium acetate/isopropanol precipitation and was resuspended in 15 µl of formamide loading dye.

Mapping of CRD-BP-binding sites using hydroxyl radical foot-printing

The Fe(II)/EDTA cleavage complex (36) was used to map the CRD-BP-binding sites on c-*myc* CRD-1705-1886. Initially, binding between c-*myc* CRD (~45 nM; 100 000 c.p.m./reaction) and CRD-BP (1500 nM) was facilitated using the standard EMSA buffer and reaction conditions as described above. Immediately following the binding reaction, 6 µl of Fe(II)/EDTA cleavage reagent (0.4 mM $Fe(II)(NH_4)_2(SO_4)_2$, 0.8 mM EDTA pH 8.0, 20 mM L-ascorbic acid sodium salt, 0.35% H_2O_2) was added to the 20 µl binding reaction. The cleavage reaction was incubated at room temperature for 10 min and was terminated by the addition of 5 µl 0.1 M Thiourea (Sigma). The RNA was extracted by ammonium acetate/isopropanol precipitation and the pellet was resuspended in 15 µl formamide loading dye. About 5 µl of the reaction was run on an 8% denaturing polyacrylamide-sequencing gel.

RESULTS

Purified recombinant His_6-tagged CRD-BP binds to the full-length c-*myc* CRD RNA nts 1705–1886 and *MDR*-1 RNA nts 746–962

In an effort towards testing the CRD-BP-c-*myc* CRD shielding hypothesis, it was imperative to demonstrate that purified recombinant His_6-tagged CRD-BP could bind avidly to the CRD. The plasmid pET28b(+)-CRD-BP was used to generate the recombinant mouse CRD-BP containing a His_6-tag at the C-terminus of the protein. CRD-BP fractions eluted from the Ni-NTA column contained an enriched band at ~68 kDa when visualized by SDS-PAGE, (refer to lane 3, Figure 1) which is consistent with the predicted and reported molecular weight of recombinant mouse CRD-BP (13). The recombinant His_6-tagged CRD-BP of ~95% purity was consistently obtained and an example of this is shown in lane 3, Figure 1. Additional recombinant proteins, Rpp20, Rpp21, Rpp25 and Rpp40, were used as controls in this investigation. Rpp20, Rpp21, Rpp25 and Rpp40 are protein subunits of human RNase P (32–34) and were chosen on the basis of their ability or inability to bind to nucleic acids. The criteria used to determine if these recombinant proteins possessed this binding potential was based on the presence of putative nucleic-acid-binding domains in their sequence and known RNA–protein interactions. Purity of the recombinant proteins was assessed by visualization using Coomasie blue-stained SDS-PAGE. As shown in Figure 1, the purity of all the recombinant proteins was greater than 95% and their observed molecular weights were consistent with their predicted molecular weights (lanes 2, 4, 5, 7).

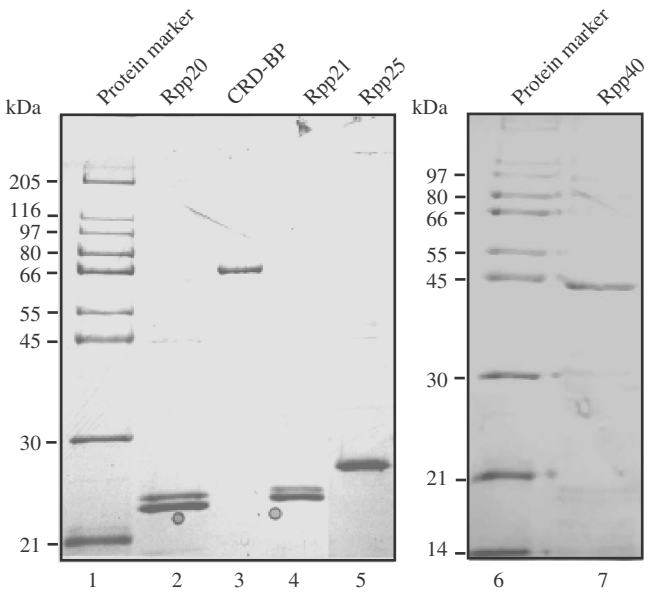

Figure 1. Analysis of purified recombinant His_6-tagged proteins by SDS-PAGE. Recombinant His_6-tagged mouse CRD-BP was purified using Ni-NTA spin column and dialyzed prior to separation (2 µg) (lane 3) on 12% SDS-PAGE and visualization by Coomasie blue staining. Recombinant His_6-tagged human Rpp20 (lane 2), Rpp21 (lane 4), Rpp25 (lane 5) and Rpp40 (lane 7) were also purified and dialyzed in a similar manner before its purity (2 µg) being analyzed on Coomasie blue-stained SDS-PAGE.

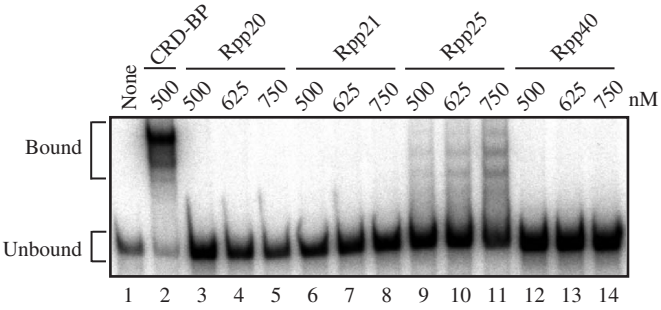

Figure 2. Electromobility shift assay showing binding of recombinant CRD-BP and Rpp25 to c-*myc* CRD RNA. About 500 nM of purified recombinant CRD-BP (lane 2) and purified recombinant Rpp20 (lanes 3–5), Rpp21 (lanes 6–8), Rpp25 (lanes 9–11) and Rpp40 (lanes 12–14) (at various concentrations as indicated) were incubated with 40 nM [^{32}P] c-*myc* CRD RNA nts 1705–1886 (~50 000 c.p.m). None (lane 1) indicates no protein was added. The positions of protein–RNA complexes (Bound) and unbound RNA (Unbound) are indicated on the left.

EMSA was performed to determine whether the purified and dialyzed recombinant proteins were capable of binding to c-*myc* CRD RNA nts 1705–1886. About 500 nM recombinant CRD-BP was incubated with c-*myc* CRD [^{32}P]RNA and RNA–protein complexes were visualized following non-denaturing gel electrophoresis. As shown in lane 2, Figure 2, two clear bound complexes

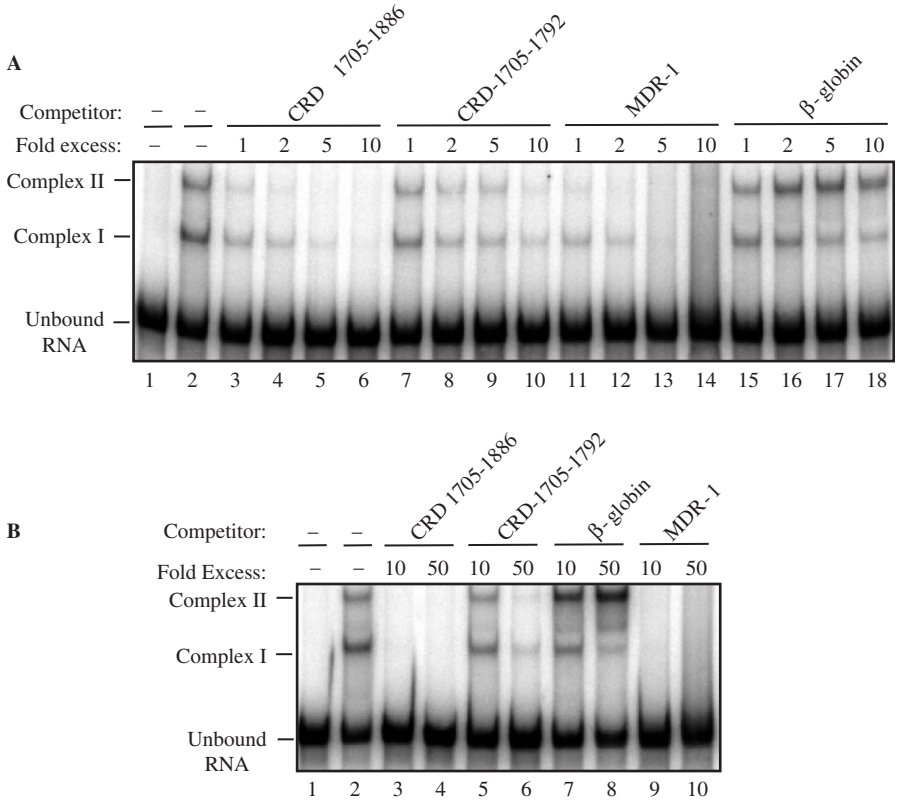

Figure 3. Electromobility shift competition assays with c-*myc* CRD RNA, β-*globin* RNA or *MDR*-1 RNA. About 350 nM of purified recombinant His_6-tagged CRD-BP was incubated with 40 nM [^{32}P] c-*myc* CRD RNA nts 1705–1886 (50 000 c.p.m) with or without the indicated molar excess of unlabeled competitor RNA. (**A**) 1–10 molar excess of unlabeled c-*myc* CRD RNA nts 1705–1886 (lanes 3–6), c-*myc* CRD RNA nts 1705–1792 (lanes 7–10), *MDR*-1 RNA nts 746–962 (lanes 11–14) and β-*globin* RNA nts 1–145 (lanes 15–18) were used. (**B**) 10–50 molar excess of unlabeled c-*myc* CRD RNA nts 1705–1886 (lanes 3 and 4), c-*myc* CRD RNA nts 1705–1792 (lanes 5 and 6), β-*globin* RNA nts 1–145 (lanes 7 and 8) and *MDR*-1 RNA nts 746–962 (lanes 9 and 10) were used.

were observed. In contrast, no bound complexes were observed when 500–750 nM Rpp20 (lanes 3–5), Rpp21 (lanes 6–8) or Rpp40 (lanes 12–14) were incubated with c-*myc* CRD [^{32}P]RNA. Three low-activity binding complexes were observed when Rpp25 was incubated with c-*myc* CRD [^{32}P]RNA (lanes 9–11). The ability of Rpp25 to bind to the c-*myc* CRD was not surprising given the fact that it possesses an Alba RNA-binding motif (37,38) and it is known to bind to several RNA targets including a 71-nt segment of *H*1 RNA, *M*1 RNA and *E. coli* $tRNA^{tyr}$ (34). It should be noted that the intensity of the Rpp25-binding complexes is significantly less than CRD-BP-binding complexes at the same concentration. Further study would be required to determine if Rpp25 has in fact lower affinity than CRD-BP for c-*myc* CRD or yeast tRNA present in the EMSA reaction actually competed with Rpp25 for binding to the transcript. The inability of Rpp40 to bind with the c-*myc* CRD was supported by the previous suggestions that this protein in isolation does not play a role in nucleic acid binding (37,38).

To further determine if the recombinant CRD-BP-c-*myc* CRD [^{32}P] RNA nts 1705–1886 association was specific, we chalenged the interaction with unlabeled competitor RNA. Our EMSA competition assays revealed that up to 50X molar excess of unlabeled β-*globin* competitor RNA was unable to dilute the binding between CRD-BP and [^{32}P] c-*myc* CRD (lanes 15–18, Figure 3A; lanes 7–8, Figure 3B). The inability of unlabeled β-*globin* competitor to dilute the CRD-BP-c-*myc* CRD interaction in conjunction with the saturation-binding experiment shown in Figure 4C support the observation that the 145-nt β-*globin* RNA fragment is not a *bona fide* CRD-BP target *in vitro*. The β-*globin* results from this investigation are also supported by the two earlier reports (12,13).

Similar to unlabeled c-*myc* CRD nts 1705–1886 (compare lane 3 to lane 2, Figure 3A), at 1× molar excess, the *MDR*-1 RNA nts 746–962 was capable of diluting the CRD-BP-[^{32}P] c-*myc* CRD interaction (compare lane 11 to lane 2, Figure 3A) and at 5×, 10× and 50× molar excess it diluted the interaction completely (compare lanes 13–14 with lane 2, Figure 3A; compare lanes 9–10 with lane 2, Figure 3B). Similar results were observed when the unlabeled competitor c-*myc* CRD-1705-1886 RNA was used (compare lanes 5–6 with lane 2, Figure 3A; compare lanes 3–4 with lane 2, Figure 3B). The unlabeled competitor c-*myc* CRD nts 1705–1792 was also observed to dilute the interaction when a minimum of 2× molar excess was added (compare lane 8 to lane 2, Figure 3A) and even at 50× molar excess, the CRD-BP-[^{32}P] c-*myc* CRD interaction was still visible (compare lanes 5–6 with lane 2, Figure 3B). This result is consistent with previous observation that c-*myc* CRD nts

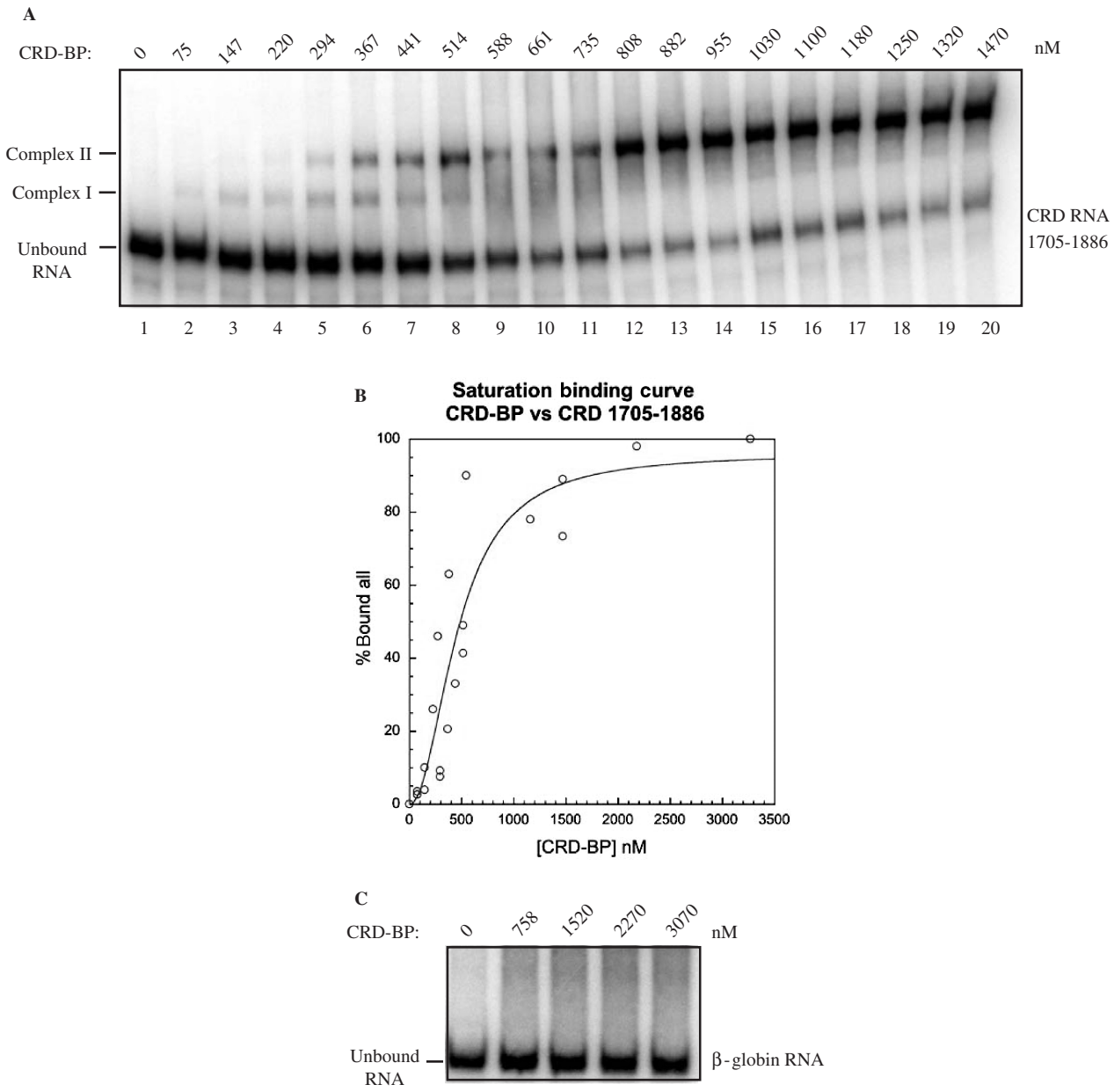

Figure 4. CRD-BP-binding affinity for c-*myc* CRD RNA and β-*globin* RNA. (**A**) An electromobility shift assay showing binding to [^{32}P] c-*myc* CRD RNA nts 1705–1886 by an increasing amount of purified recombinant His_6-tagged CRD-BP (0–1470 nM). (**B**) Binding activity in (**A**) was quantified using the PhorphorImager to compare the relative amount of radiolabeled unbound RNA shifted into slower-migrating Complex I and Complex II. Data obtained was then used to plot the saturation binding curve as shown. (**C**) An electromobility shift assay assessing the ability to bind to [^{32}P] β-*globin* RNA nts 1–145 by an increasing amount of purified recombinant His_6-tagged CRD-BP (0–3070 nM).

1705–1792 has indeed reduced affinity for CRD-BP as compared to the full-length c-*myc* CRD nts 1705–1886 (13). It is possible that the secondary structure of the c-*myc* CRD-1705-1886 contains the full complement of recognition and binding elements that facilitate high-affinity-binding interactions with CRD-BP.

Characterizing the binding of CRD-BP to c-*myc* CRD RNA and *MDR*1 RNA

Although CRD-BP is known to bind to the c-*myc* CRD (12,13), the binding characteristics between the two components has not been previously determined. With the availability of purified recombinant CRD-BP as well as *MDR*-1 RNA, we decided to further characterize and compare the nature of the binding interactions. Saturation-binding experiments were carried out using the standard EMSA conditions and employed a wide range of CRD-BP concentrations. The saturation-binding experiments were conducted three times, using three different purified CRD-BP preparations. A representative result for the binding of CRD-BP to c-*myc* [^{32}P] CRD RNA nts 1705–1886 is shown in Figure 4A. It was determined experimentally that the minimum concentration of

CRD-BP required to generate Complex I (binding of one molecule of CRD-BP, see below for discussion) was about 15 nM (data not shown). At concentrations above 100 nM, the slower migrating Complex II (binding of two molecules of CRD-BP, see below for discussion) was frequently observed (lanes 3–20, Figure 4A). In many instances, at higher concentrations of CRD-BP (e.g. 500–750 nM), Complex I was absent and it would appear that the bound RNA shifted exclusively to Complex II (compare lanes 8–20 to lanes 2–7, Figure 4A). When the saturation-binding data from Figure 4A was fit to the Hill equation and expressed graphically, a sigmoidal curve was generated as shown in Figure 4B (K_d of 500 nM). It is important to point out that the concentration of CRD-BP at which formation of Complexes I and II would take place was highly dependent upon the age of the dialyzed protein and the number of freeze–thaw cycles subjected to the protein. However, the actual dissociation constant may be lower than 500 nM because it cannot be assumed that 100% of the CRD-BP molecules were present in a conformation suitable for binding.

Keeping in mind the limitation of the EMSA, we also performed saturation-binding experiments to determine if CRD-BP could bind with other radiolabeled RNA substrates. When challenged with [^{32}P] β-*globin* RNA, CRD-BP up to 3070 nM was unable to form an observable RNA–protein complex (Figure 4C). However, when CRD-BP was challenged with [^{32}P] *MDR*-1, two RNA–protein complexes that exhibited a similar profile to that of the CRD-BP-c-*myc* CRD interaction were observed; $K_d = 500$ nM (Figure 5). The analysis of the combined binding data from three separate experiments revealed a level of cooperativity was present between the formation of the first and second binding complexes (Figure 5B). The cooperativity observed is also reflected in the Hill coefficient, which for CRD-BP versus c-*myc* CRD (Figure 4B) was 2.06, and 2.6 when challenged with *MDR*-1 RNA (Figure 5B). The Hill coefficients in both cases suggest that two molecules of CRD-BP bind with one molecule of c-*myc* CRD RNA or with one molecule of *MDR*-1 RNA at identical or non-identical sites. Evidence to support a two RNA-binding site model is provided by the kinetic analysis of the interactions between IMP-1 and *IGF*-II RNA (39). In this study, IMP-1 was shown to bind through a cooperative, sequential mechanism via two binding sites within the *IGF*-II transcript (39). Interestingly, dissociation constant of about 2 nM was reported for the interaction between IMP-1 and *IGF*-II RNA (39). The significantly higher dissociation constant determined in this study could reflect the inefficiency of renaturation of CRD-BP and c-*myc* CRD RNA as discussed above, or/and the use of His_6-tagged CRD-BP since it has been previously reported that tagged-IMP-1 exhibited poor RNA binding (14).

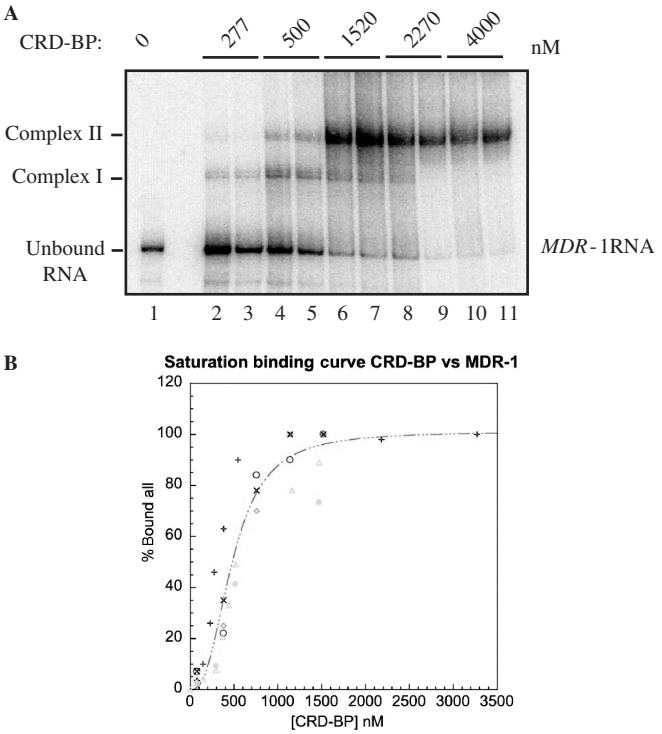

Figure 5. CRD-BP binding affinity for *MDR*-1 RNA. (**A**) An electromobility shift assay showing binding to [^{32}P] *MDR*-1 RNA nts 746–962 by an increasing amount of purified recombinant His_6-tagged CRD-BP (0–4000 nM). (**B**) Binding activity in (**A**) was quantified using the PhorphorImager to compare the relative amount of radiolabeled unbound RNA shifted into slower-migrating Complex I and Complex II. Data obtained from three separate experiments was then used to plot the saturation binding curve as shown.

CRD-BP protects the c-*myc* CRD and *MDR*-1 RNA from cleavage by the mammalian endoribonuclease

Having established that recombinant CRD-BP can bind c-*myc* CRD and *MDR*-1 RNA, we then sought to determine if the binding of CRD-BP to RNA could directly protect these transcripts from degradation by an endoribonuclease recently discovered in our lab (31).

5′-End labeled c-*myc* CRD nts 1705–1886 was incubated with one unit of the purified endonuclease in the presence or absence of recombinant CRD-BP. As shown in Figure 6A, the typical ten distinct cleavage sites at nts 1742, 1747, 1751, 1757, 1768, 1771, 1773, 1775, 1845 and 1855 were generated upon incubation with the purified endonuclease (lanes 3, 8 and 13) (31). For ease in quantification and categorization, we have named the separate cleavage sites as Region I (1845, 1855), Region II (1768, 1771, 1773, 1775) and Region III (1742, 1747, 1751, 1757) (Figure 6). Incubation of the transcript with recombinant CRD-BP at 500 nM (lane 2), 750 nM (lane 7) and 1500 nM (lane 12) alone had no effect, indicating that CRD-BP lacks RNase activity. It was anticipated that c-*myc* cleavage would be reduced using CRD-BP concentrations equal to the measured dissociation constant because 50% of c-*myc* CRD would be bound at 500 nM (Figure 4A and B). This prediction was confirmed by the reduction in cleavage fragments observed in all three regions indicated in Figure 6A (compare lanes 4–5 with lane 3). At 500 nM, CRD-BP was responsible for a 43% reduction in Region I, a 72% reduction in Region II and a 77% reduction in Region III.

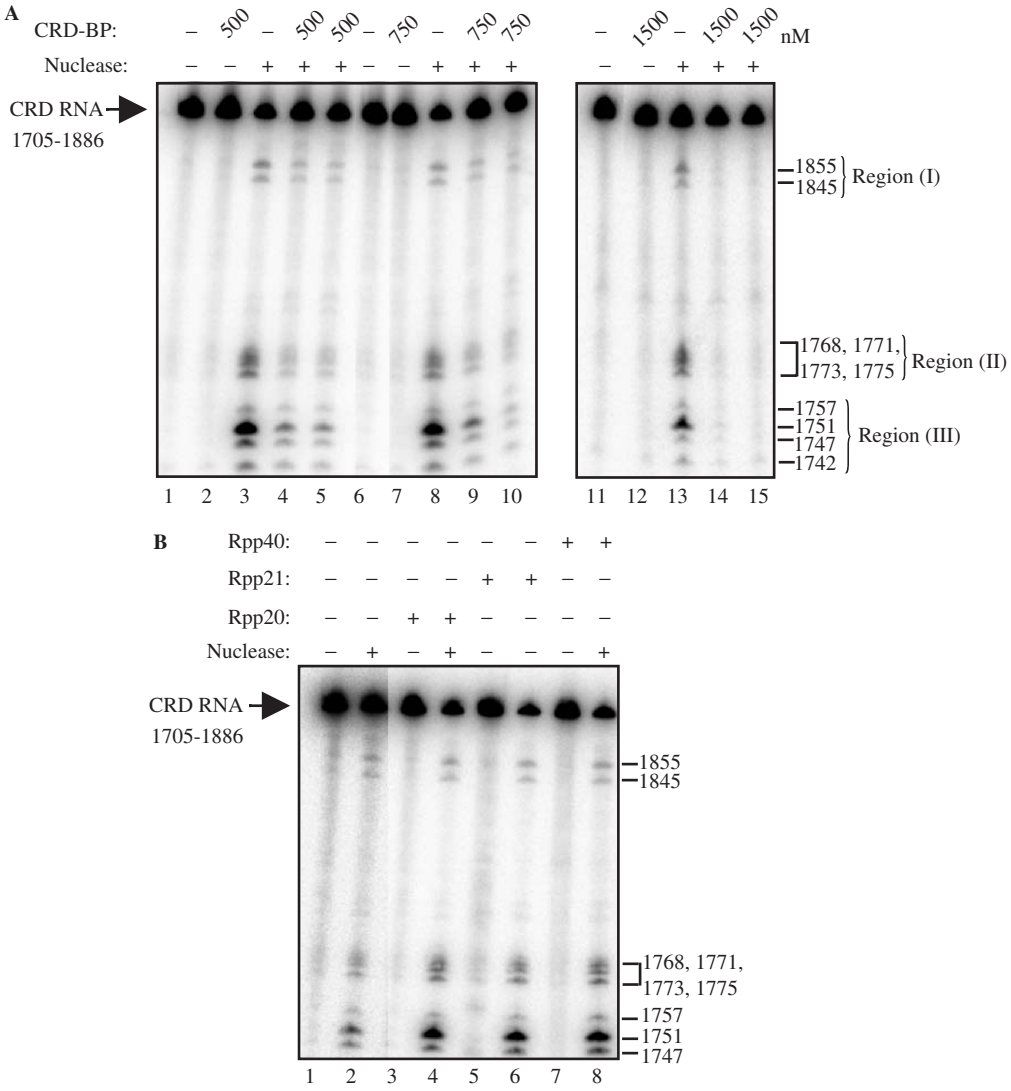

Figure 6. CRD-BP shields the c-*myc* CRD RNA from endonucleolytic attack by a mammalian endoribonuclease. (**A**) One unit of the purified mammalian endoribonuclease was incubated with [^{32}P] c-*myc* CRD RNA nts 1705–1886 as described in the Materials and methods section, with (lanes 4, 5, 9, 10, 14, 15) or without (lanes 3, 8 and 13) the presence of 500, 750 or 1500 nM of purified recombinant His_6-tagged CRD-BP as shown. (**B**) As in (**A**), the purified endoribonuclease was incubated with the radiolabeled c-*myc* CRD RNA in the absence (lane 2) or presence of 1500 nM of Rpp20 (lane 4), Rpp21 (lane 6) and Rpp40 (lane 8). Lanes 3, 5 and 7 had the purified recombinant proteins only. Numbers on the right indicate the cleavage sites generated by the mammalian endoribonuclease on the CRD RNA substrates.

It was predicted that cleavage reductions would increase at concentrations above the measured dissociation constant because at 750 and 1500 nM, ~75 and 90% of c-*myc* CRD were bound by CRD-BP respectively (Figure 4A and B). At 750 nM, (lanes 9–10, Figure 6A) CRD-BP was responsible for a 45% reduction in Region I, a 75% reduction in Region II and a 80% reduction in Region III. As shown in lanes 14–15 in Figure 6A, at 1500 nM, CRD-BP was responsible for the 95% cleavage reductions observed in all three regions.

To determine if the blocking effect was due to specific binding interactions, we incubated c-*myc* CRD RNA with Rpp20, Rpp21 and Rpp40 which had been shown to have no affinity for the transcript (Figure 2). Figure 6B shows that at 1500 nM, Rpp20, Rpp21 and Rpp40 were unable to block endonucleolytic cleavage of CRD RNA by the native mammalian endoribonuclease (compare lanes 4, 6 and 8 to lane 2).

CRD-BP was shown to bind with considerable affinity and specificity to *MDR*-1 RNA (Figure 5) and we have previously shown that the endonuclease is capable of cleaving *MDR*-1 RNA (31). It was therefore anticipated that CRD-BP would also be capable of blocking *MDR*-1 cleavage by the mammalian endoribonuclease. As predicted, CRD-BP was observed to shield *MDR*-1 RNA from endonucleolytic attack in a concentration-dependent manner (Figure 7A), and the most significant cleavage reductions were observed at 1500 nM (lane 3, Figure 7A). The consistent reduction observed in all regions suggests that the entire *MDR*-1 RNA was protected via CRD–BP interactions. We have also tested the ability of CRD-BP to block cleavage of β-*globin* RNA by the endonuclease.

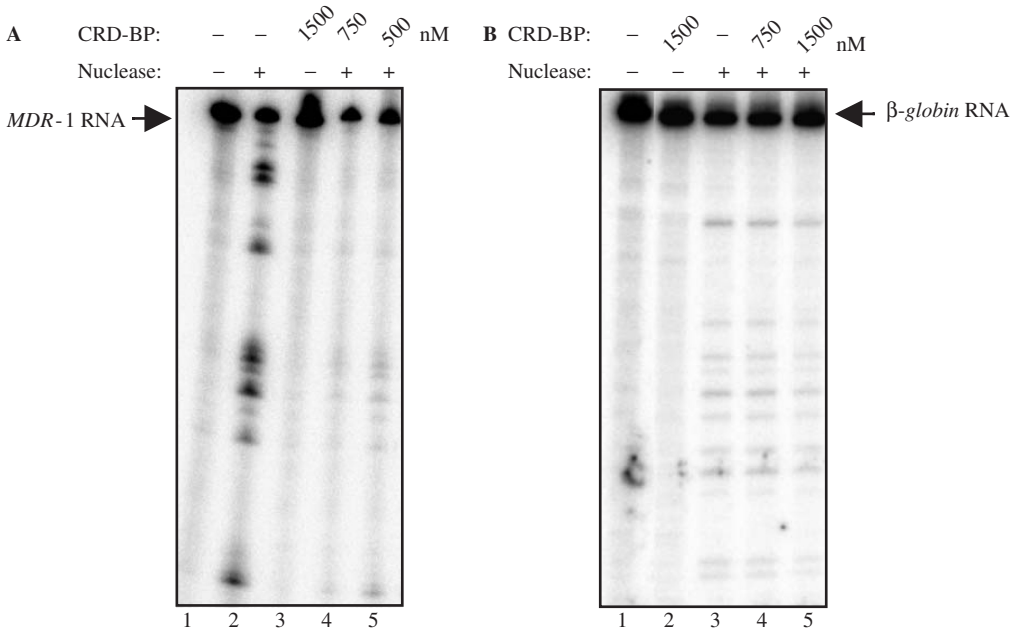

Figure 7. CRD-BP is capable of shielding *MDR*-1 RNA from endonucleolytic attack by the mammalian endoribonuclease. **(A)** One unit of the purified mammalian endoribonuclease was incubated with [^{32}P] *MDR*-1 RNA nts 746–962 as described in the Materials and methods section, without (lane 2) or with the presence of 500 nM (lane 5), 750 nM (lane 4) or 1500 nM (lane 3) of purified recombinant His_6-tagged CRD-BP. Lane 2 had the input RNA only. **(B)** As in (**A**), the purified endoribonuclease was incubated with [^{32}P] β-*globin* RNA nts 1–145 without (lane 3) or with the presence of 750 nM (lane 4) or 1500 nM (lane 5) of purified recombinant His_6-tagged CRD-BP. Lane 1 had the input RNA only.

As expected, CRD-BP that had no affinity for β-*globin* RNA (Figure 4C) did not effectively block the endonuclease from cleaving this transcript (Figure 7B).

Taken together, our overall results suggest that CRD-BP was capable of shielding both c-*myc* CRD and *MDR*-1 RNAs in a dose-dependent manner from the cleavage activities of a mammalian endoribonuclease via specific RNA–protein interactions. In addition, the results suggest that CRD-BP binds to a considerable portion of both *MDR*-1 and c-*myc* RNAs and at 1500 nM, both RNA transcripts appeared to be entirely protected.

Mapping the CRD-BP-binding sites on c-*myc* CRD RNA

To map the CRD-BP-binding sites on c-*myc* CRD, we used the hydroxyl radical foot-printing method (36). The chemical cleavage reagent chosen was the Fe(II)/EDTA complex. The Fe(II)/EDTA complex is a negatively charged species and does not interact electrostatically with the RNA molecule thereby limiting its interference with RNA–protein interactions (36). The complex is known to generate hydroxyl radicals from the reduction of hydrogen peroxide in a reaction known as the Haber–Weiss reaction (36). The hydroxyl radical is thought to cleave the RNA backbone by attacking ribose moieties (36). Regions of the RNA backbone that are occluded by protein are cleaved with decreased efficiency by the radical and the result is a series of cleavage fragments exhibiting reduced intensity (36).

Figure 8A shows a typical CRD-BP-c-*myc* CRD foot-printing experiment. Lane 3 depicts the Fe(II)/EDTA cleavage profile characteristic of [^{32}P] c-*myc* CRD-1705–1886 in the absence of CRD-BP. The alkaline hydrolysis ladder (lane 2) exhibited a uniform cleavage profile with the exception of two enriched fragments located between nts 1794 and 1842; which were also observed in lanes 4–9. RNase T1 digest of [^{32}P] c-*myc* CRD-1705–1886 shown in lane 1 provided mapping for cleavage site identification. The cleavage pattern observed as a result of Fe(II)/EDTA-treatment of c-*myc* CRD was hallmarked by several enriched fragments which have been mapped and are indicated in Figure 8A. When compared to cleavage reactions containing 1500 nM CRD-BP (lanes 4–7), it is apparent that several regions of cleavage were significantly reduced. The cleavage fragments corresponding to nts 1741 and 1748 (lane 3) were reduced by 75%. An equivalent reduction was also observed at discrete fragments in the nucleotide region spanning 1765–1775 (compare lane 3 with lanes 4–7). At positions 1787 and 1791, a 50% reduction in cleavage intensity was observed and a 75% reduction was also observed at positions 1843, 1855 and 1864 (compare lane 3 with lanes 4–7). Figure 8B shows the identified CRD-BP-binding sites in comparison with the putative CRD-BP-binding sites previously determined using antisense oligonucleotides (29). Six of the binding sites (1765, 1767, 1771, 1773, 1775, 1787) identified in this study were in good agreement with those identified by Coulis *et al.* (29). Six identified CRD-BP-binding sites (1747, 1767, 1771, 1773, 1855) are within the direct cleavage sites of the mammalian endonuclease and five (1741, 1765, 1787, 1791, 1843) are within one to two nucleotides away from the enzyme cleavage sites (Figure 8B). Such observation is consistent with the notion that CRD-BP is capable of shielding c-*myc* CRD RNA from attack by the endonuclease.

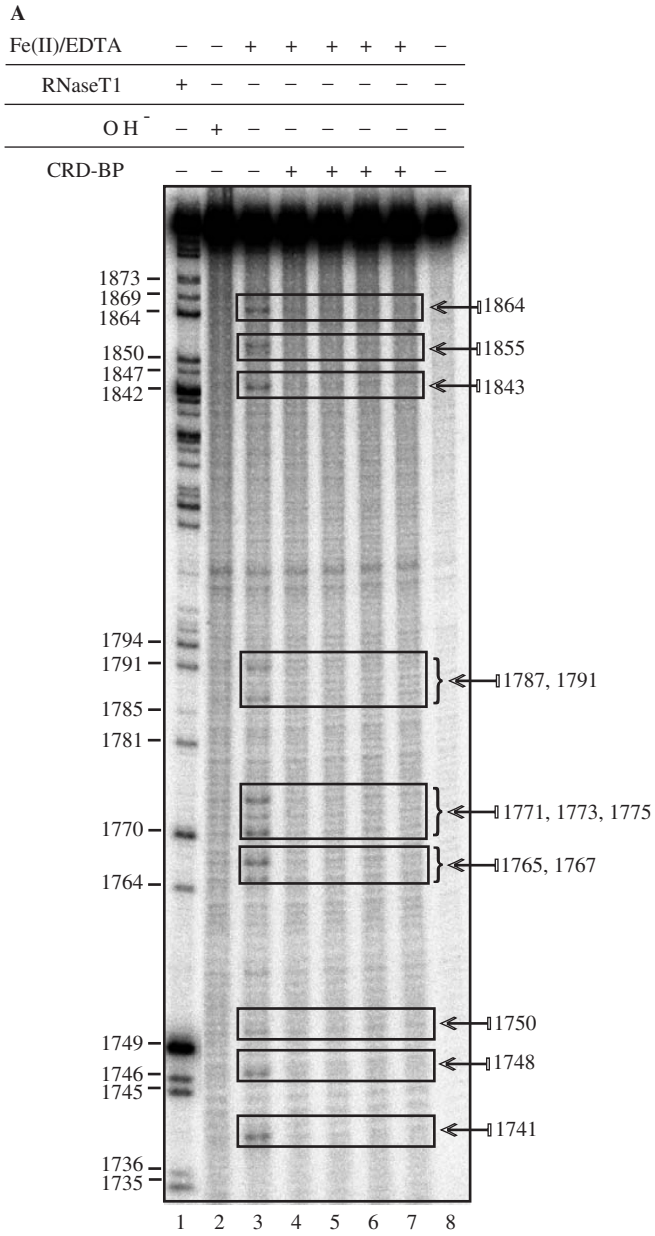

Figure 8. Mapping of CRD-BP-binding sites on c-*myc* CRD RNA using the hydroxyl radical-mediated cleavage reaction. **(A)** 45 nM [^{32}P] c-*myc* CRD RNA nts 1705–1886 was subjected to Fe(II)/EDTA cleavage reaction in EMSA-binding buffer in the absence (lane 3) or presence (lanes 4–7) of 1500 nM purified recombinant His_6-tagged CRD-BP. Reaction samples were run on a 8% denaturing polyacrylamide gel, fixed, dried and subjected to autoradiography as described in the Materials and methods section. Lane 8 is the input RNA. Lanes 1 and 2 represent RNase T1 digest and alkaline hydrolysis of the radiolabeled c-*myc* CRD RNA respectively. Regions highlighted by rectangles showed significant reductions in cleavage. Numbers on the left indicate guanosine cleavage sites of RNase T1 digest and numbers on the right indicate the hydroxyl radical-mediated cleavage sites. **(B)** Identified CRD-BP-binding sites on sequences of c-*myc* CRD RNA nts 1705–1886. Underlined sequences indicate the CRD-BP-binding sites as determined by the hydroxyl radical foot-printing in (**A**). Bolded sequences indicate the putative CRD-BP-binding sites as previously determined using antisense oligonucleotides competition method (29). Arrows indicate cleavage sites generated by the purified endoribonuclease (31).

DISCUSSION

CRD-BP belongs to the VICKZ family of RNA-binding proteins that influence various aspects of cellular physiology such as cell growth and differentiation (40). CRD-BP was initially discovered (5) and eventually purified (12) based on its ability to bind to the c-*myc* CRD. The working model for CRD-BP function is that it binds to and protects the c-*myc* CRD from endonucleolytic cleavage, resulting in enhanced transcript half-life and expression (5). This hypothesis is supported by evidence from *in vitro* mRNA decay studies (5,12) as well as studies in cells (3,28). Although this hypothesis has been proposed for a number of years, it has not been directly tested. That is CRD-BP has not been directly

shown to block CRD cleavage by an endoribonuclease. This is in part due to the unavailability of a candidate endoribonuclease that can cleave within the c-*myc* CRD. In this study, we show that recombinant CRD-BP can dose-dependently inhibit cleavage of c-*myc* CRD and *MDR*-1 RNA by a mammalian endoribonuclease. This blocking effect correlates with CRD-BP's dose-dependent affinity for c-*myc* CRD and *MDR*-1 RNAs.

Specificity of recombinant CRD-BP for the CRD was demonstrated in two ways. First, while three other recombinant proteins, Rpp20, Rpp21 and Rpp40, had no affinity for c-*myc* CRD, CRD-BP was shown to bind strongly to the transcript (Figure 2). Second, consistent with previous findings (12,13), c-*myc* CRD competitor RNAs were effective in competing with [^{32}P]c-*myc* CRD in binding to CRD-BP, with nts 1705–1886 being more effective than nts 1705–1792 (Figure 3). On the contrary, at 50× molar excess, β-*globin* RNA could not compete with [^{32}P]c-*myc* CRD in binding to CRD-BP. Unexpectedly, we found that the coding region of *MDR*-1 RNA nts 746–962 was as effective as c-*myc* CRD nts 1705–1886 in competing for binding to CRD-BP (Figure 3). This result is consistent with the observed saturating-binding profile upon incubation of excess CRD-BP with [^{32}P]*MDR*-1 RNA (Figure 5).

The K_d for the CRD-BP-c-*myc*-1705–1886 interaction was significantly lower than that of CRD-BP-c-*myc*-1705–1792 interaction. It is apparent that one of the proposed CRD-BP-binding sites (nts 1843–1864) is absent from the 1705–1792 CRD region, and may attributed to the differences in specificity and stability observed in the RNA–protein interactions. The binding profiles exhibited by the CRD-BP-c-*myc* CRD and CRD-BP–*MDR*-1 interactions were hallmarked by the presence of two binding complexes. These RNA–protein interactions are believed to occur via a sequential, cooperative binding mechanism. The formation of the faster migrating Complex I at low concentrations of CRD-BP, the emergence of the slower migrating Complex II at intermediate concentrations of CRD-BP and the predominance of Complex II at concentrations greater than (or) equal to the calculated K_d are suggestive of a sequential binding mechanism. It is possible that the formation of Complex I may represent an intermediate state in which one molecule of CRD-BP is bound to one RNA molecule. The emergence of Complex II suggests that a second molecule of CRD-BP engages in interactions with a Complex I species in a concentration-dependent manner. We propose that Complex II may function to increase the stability and specificity of the RNA–protein interaction. Such interactions have also been observed and proposed for IMP-1-*IGF*-II RNA (39) and Vg1RBP-*VLE* 3′-UTR RNA (41).

Our data demonstrated that the blocking of endonuclease-mediated c-*myc* CRD cleavage by CRD-BP is concentration dependent and this correlated with concentration-dependent binding of CRD-BP to the transcript. We propose that at 500 nM CRD-BP, most c-*myc* CRD RNA molecules are bound by only one molecule of CRD-BP. At 1500 nM CRD-BP, c-*myc* CRD RNA is likely to be bound by two molecules of CRD-BP as observed by the formation of Complex II. In this scenario, it is highly likely that the entire transcript is bound and protected by CRD-BP as evidenced by the hydroxyl radical foot-printing experiments (Figure 8). Our observations that CRD-BP binds to larger stretches of nucleotides rather than to specific positions is supported by evidence that members of the VICKZ family bind to larger elements rather than to individual nucleotides (40). Further evidence to support this came from a study using complementary oligonucleotides to map the CRD-BP-binding sites within the c-*myc* CRD (29). Our findings of the presence of CRD-BP-binding sites within the regions targeted by the mammalian endoribonuclease support the hypothesis that CRD-BP serves as a stabilizing factor for c-*myc in vitro*. The evidence provided in this study confirms that CRD-BP is in fact capable of blocking a mammalian endoribonuclease from cleaving c-*myc* CRD via specific interactions with RNA sequences.

To our knowledge, this is the first study to demonstrate the ability of CRD-BP to directly protect c-*myc* CRD cleavage by an endoribonuclease. This is a critical first step towards directly testing the interaction between CRD-BP and endoribonuclease in regulating c-*myc* CRD cleavage in cells. As indicated in the Introduction, four studies indirectly supported this hypothesis (18,27,28,29). However, two recent observations on the lack of changes in c-*myc* mRNA and protein levels upon changes in CRD-BP expression (21,30) are inconsistent with this working model. As previously suggested (21,30), the known multilevel regulation of c-*myc* gene expression could contribute to these observations. Alternatively, the absence of the responsible endoribonuclease may in part explain these unexpected findings. The latter hypothesis can be investigated upon availability of identified endoribonucleases that can cleave within the c-*myc* CRD.

Our finding that CRD-BP has high affinity for *MDR*-1 RNA was totally unexpected and has important implications. *MDR*-1 is a plasma membrane drug-transporter protein and is associated with multidrug resistance phenotypes in cultured cells as well as in human cancers (42). Enhanced mRNA stability for *MDR*-1 and c-*myc* mRNA has been reported in liver cancer (43) and *MDR*-1 mRNA decay intermediates corresponding to nts 746–962 of *MDR*-1 have been detected in the normal liver but not liver cancer (44). Although CRD-BP expression has not been studied in liver cancer, results to date are consistent with the model that c-*myc* and *MDR*-1 mRNAs are short-lived in normal adult tissues (43) because CRD-BP is absent or present at low levels. However, in cancerous liver cells, enhanced *MDR*-1 and c-*myc* mRNAs (43) are observed because CRD-BP may be overexpressed.

In conclusion, our data provides direct evidence that CRD-BP can indeed protect c-*myc* mRNA from cleavage by an endoribonuclease, and supports its proposed role in regulating mRNA stability in cells. We have also identified *MDR*-1 RNA as a new target for CRD-BP, and the transcript can also be protected from endonucleolytic cleavage by CRD-BP. These findings provided

further support for the significant and global roles that CRD-BP play in regulating mRNA stability in cancer.

ACKNOWLEDGEMENTS

This work was supported by a grant from Natural Science & Engineering Research Council and Canadian Liver Foundation. C.H.L. is a Research Scientist of the National Cancer Institute of Canada supported with funds provided by the Canadian Cancer Society. We thank Andrea Gorrell for her assistance in the preparation of saturation-binding curves. Funding to pay the Open Access publication charge was provided by the NSERC Discovery Grant 227158.

Conflict of interest statement. None declared.

REFERENCES

1. Levens,D. (2003) Reconstructing MYC. *Genes Dev*., **17**, 1071–1077.
2. Nesbit,C.E., Tersak,J.M. and Prochownik,E.V. (1999) MYC oncogenes and human neoplastic disease. *Oncogene*, **18**, 3004–3016.
3. Herrick,D.J. and Ross,J. (1994) The half-life of c-*myc* mRNA in growing and serum-stimulated cells: influence of the coding and 3′ untranslated regions and role of ribosome translocation. *Mol. Cell. Biol*., **14**, 2119–2128.
4. Shiu,R.P.C., Watson,P.H. and Dubik,D. (1993) C-*myc* oncogene expression in estrogen-dependent and -independent breast cancer. *Clin. Chem*., **39**, 353–355.
5. Bernstein,P.L., Herrick,D.J., Prokipcak,R.D. and Ross,J. (1992) Control of c-*myc* mRNA half-life *in vitro* by a protein capable of binding to a coding region determinant. *Genes Dev*., **6**, 642–654.
6. Brewer,G. (1999) Evidence for a 3′-5′ decay pathway for c-*myc* mRNA in mammalian cells. *J. Biol. Chem*., **274**, 16174–16179.
7. Brewer,G. (2000) Regulation of c-myc mRNA decay *in vitro* by a phorbol ester-inducible, ribosome-associated component in differentiating megakaryoblasts. *J. Biol. Chem*., **275**, 33336–33345.
8. Lemm,I. and Ross,J. (2002) Regulation of c-myc mRNA decay by translational pausing in a coding region instability determinant. *Mol. Cell. Biol*., **22**, 3959–3969.
9. Morello,D., Lavenu,A., Pournin,S. and Babinet,C. (1993) The 5′ and 3′ non-coding sequences of the c-*myc* gene, required in vitro for its post-transcriptional regulation, are dispensable *in vivo*. *Oncogene*, **8**, 1921–1929.
10. Wisdom,R. and Lee,W. (1991) The protein coding region of c-*myc* mRNA contains a sequence that specifies rapid mRNA turnover and induction by protein synthesis inhibitor. *Genes Dev*, **5**, 232–243.
11. Yielding,N.M. and Lee,W.M.F. (1997) Coding elements in exons 2 and 3 target c-*myc* mRNA downregulation during myogenic differentiation. *Mol. Cell. Biol*., **17**, 2698–2707.
12. Prokipcak,R.D., Herrick,D.J. and Ross,J. (1994) Purification and properties of a protein that binds to the C-terminal coding region of human c-*myc* mRNA. *J. Biol. Chem*., **269**, 9261–9269.
13. Doyle,G.A.R., Betz,N.A., Leeds,P.L., Fleisig,A.J., Prokipcak,R.D. and Ross,J. (1998) The c-*myc* coding region determinant-binding protein: a member of a family of KH domain RNA-binding proteins. *Nucleic Acid Res*., **26**, 5036–5044.
14. Nielsen,J., Christiansen,J., Lykke-Andersen,J., Johnsen,A.H., Wewer,U.M. and Nielsen,F.C. (1999) A family of insulin-like growth factor II mRNA-binding proteins represses translation in late development. *Mol. Cell. Biol*., **19**, 1262–1270.
15. Leeds,P., Kren,B.T., Boylan,J.M., Betz,NA., Steer,C.J., Gruppuso,P.A. and Ross,J. (1997) Developmental regulation of CRD-BP, an RNA-binding protein that stabilizes c-*myc* mRNA *in vitro*. *Oncogene*, **14**, 1279–1286.
16. Hansen,T.V.O., Hammer,N.A., Nielsen,J., Madsen,M., Dalbaeck,C., Wewer,U.M. and Christiansen,J. (2004) Dwarfism and impaired gut development in insulin-like growth factor II mRNA-binding protein 1-deficient mice. *Mol. Cell. Biol*., **24**, 4448–4464.
17. Ioannidis,P., Mahaira,L., Papaioannou,D., Teixera,M.R., Heim,S., Andersen,J.A., Evangelou,E., Dafni,U., Pandis,N. *et al*. (2003) 8q24 Copy number gains and expression of the c-*myc* mRNA stabilizing protein *CRD-BP* in primary breast carcinomas. *Int. J. Cancer*, **104**, 54–59.
18. Ross,J., Lemm,I. and Berberet,B. (2001) Overexpression of an mRNA-binding protein in human colorectal cancer. *Oncogene*, **20**, 6544–6550.
19. Ioannidis,P., Kottaridi,C., Dimitriadis,E., Courtis,N., Mahaira,L., Talieri,M., Giannopoulos,A., Iliadis,K., Papaioannou,D. *et al*. (2004) Expression of the RNA-binding protein CRD-BP in brain and non-small cell lung tumors. *Cancer Lett*., **209**, 245–250.
20. Doyle,G.A., Bourdeau-Heller,J.M., Coulthard,S., Meisner,L.F. and Ross,J. (2000) Amplification in human breast cancer of a gene encoding a c-*myc* mRNA-binding protein. *Cancer Res*., **60**, 2756–2759.
21. Tessier,C.R., Doyle,G.A., Clark,B.A., Pitot,H.C. and Ross,J. (2004) Mammary tumor induction in transgenic mice expressing an RNA-binding protein. *Cancer Res*., **64**, 209–214.
22. Nielsen,J., Nielsen,F.C., Kristenses,M.A., Koch,G. and Christiansen,J. (2002) Cytoplasmic trafficking of IGF-II mRNA-binding protein by conserved KH domains. *J. Cell Sci*., **115**, 2087–2097.
23. Runge,S., Nielsen,F.C., Nielsen,J., Lykke-Andersen,J., Wewer,U.M. and Christiansen,J. (2000) H19 RNA binds four molecules of insulin-like growth factor II mRNA-binding protein. *J. Biol. Chem*., **275**, 29562–29569.
24. Atlas,R., Behar,L., Elliot,E. and Ginzburg,I. (2004) The insulin-like growth factor mRNA binding-protein IMP-1 and the Ras-regulatory protein G3BP associate with tau mRNA and HuD protein in differentiated P19 neuronal cells. *J. Neurochem*, **89**, 613–626.
25. Ross,A.F., Oleynikov,Y., Kislaukis,E.H., Taneja,K.L. and Singer,R.H. (1997) Characterization of a β-actin mRNA zipcode-binding protein. *Mol. Cell. Biol*., **17**, 2158–2165.
26. Vikesaa,J., Hansen,T.V.O., Jonson,L., Borup,R., Wewer,U.M., Christiansen,J. and Nielsen,F.C. (2006) RNA-binding IMPs promote cell adhesion and invadopodia formation. *EMBO J*., **25**, 1456–1468.
27. Noubissi,F.K., Elcheva,I., Bhatia,N., Shakoori,A., Ougolkov,A., Liu,J., Minamoto,T., Ross,J., Fuchs,S.Y. *et al*. (2006) CRD-BP mediates stabilization of βTrCP1 and c-*myc* mRNA in response to β-catenin signaling. *Nature*, **441**, 898–901.
28. Ioannidis,P., Mahaira,L.G., Perez,S.A., Gritzapis,A.D., Sotiropoulou,P.A., Kavalakis,G.J., Antsaklis,A.I., Baxevanis,C.N. and Papamichail,M. (2005) CRD-BP/IMP1 expression characterizes cord blood CD34+ stem cells and affects c-*myc* and IGF-II expression in MCF-7 cancer cells. *J. Biol. Chem*., **280**, 20086–20093.
29. Coulis,C.M., Lee,C., Nardone,V. and Prokipcak,R.D. (2000) Inhibition of c-*myc* expression in cells by targeting an RNA-protein interaction using antisense oligonucleotides. *Mol. Pharmacol*., **57**, 485–494.
30. Liao,B., Patel,M., Hu,Y., Charles,S., Herrick,D.J. and Brewer,G. (2004) Targeted knockdown of the RNA-binding protein CRD-BP promotes cell proliferation via insulin-like growth factor II-dependent pathway in human K562 leukemia cells. *J. Biol. Chem*., **279**, 48716–48724.
31. Bergstrom,K., Urquhart,J.C., Tafech,A., Doyle,E. and Lee,C.H. (2006) Purification and characterization of a novel mammalian endoribonuclease. *J. Cell. Biochem*., **98**, 519–537.
32. Jarrous,N., Reiner,R., Wesolowski,D., Mann,H., Guerrier-Takada,C. and Altman,S. (2001) Function and subnuclear distribution of Rpp21, a protein subunit of the human ribonucleoprotein ribonuclease P. *RNA*, **7**, 1153–1164.
33. Jarrous,N., Eder,P.S., Guerrier-Takada,C., Hoog,C. and Altman,S. (1998) Autoantigenic properties of some protein subunits of catalytically active complexes of human ribonuclease P. *RNA*, **4**, 407–417.
34. Guerrier-Takada,C., Eder,P.S., Gopalan,V. and Altman,S. (2002) Purification and characterization of Rpp25, an RNA-binding protein subunit of human ribonuclease P. *RNA*, **8**, 290–295.
35. Lawn,R.M., Efstratiadis,A., O'Connell,C. and Maniatis,T. (1980) The nucleotide sequence of the human β-*globin* gene. *Cell*, **21**, 647–651.

36. Tullius,T. and Dombroski,B.A. (1986) Hydroxyl radical footprinting: high resolution information about DNA-protein contacts and applications to lambda repressor and Cro protein. *Proc. Natl. Acad. Sci. U.S.A.*, **83**, 5469–5473.
37. Schultz,J., Copley,R.R., Doerks,T., Ponting,C.P. and Bork,P. (2000) SMART: A web-based tool for the study of genetically mobile domains. *Nucleic Acids Res.*, **28**, 231–234.
38. Jiang,T., Guerrier-Takada,C. and Altman,S. (2001) Protein-RNA interactions in the subunits of human nuclear RNase P. *RNA*, **7**, 937–941.
39. Nielsen,J., Kristensen,M.A., Willemoes,M., Nielsen,F.C. and Christiansen,J. (2004) Sequential dimerization of human zipcode-binding protein IMP1 on RNA: a cooperative mechanism providing RNP stability. *Nucleic Acids Res.*, **32**, 4368–4376.
40. Yisraeli,J.K. (2005) VICKZ proteins: a multi-talented family or regulatory RNA-binding proteins. *Biol. Cell*, **97**, 87–96.
41. Git,A. and Standart,N. (2002) The KH domains of Xenopus Vg1RBP mediate RNA binding and self-association. *RNA*, **8**, 1319–1333.
42. Ambudkar,S.V., Kimchi-Sarfaty,C., Sauna,Z.E. and Gottesman,M.M. (2003) P-glycoprotein: from genomics to mechanism. *Oncogene*, **22**, 7468–7485.
43. Lee,C.H., Bradley,G. and Ling,V. (1998) Increased P-glycoprotein messenger RNA stability in rat liver tumors *in vivo*. *J. Cell. Physiol.*, **177**, 1–12.
44. Lee,C.H., Rehaume,V.E. and Shandro,J. (2005) Identification of *in vivo* P-glycoprotein mRNA decay intermediates in normal liver but not in liver tumors. *J. Cell. Physiol.*, **204**, 638–645.